The Astrophysical Journal, 606:58–66, 2004 May 1

X-RAY EVOLUTION OF ACTIVE GALACTIC NUCLEI AND HIERARCHICAL GALAXY FORMATION

N. Menci,[1] F. Fiore,[1] G. C. Perola,[1,2] and A. Cavaliere[3]

Received 2003 September 26; accepted 2004 January 14

ABSTRACT

We have incorporated the description of the X-ray properties of active galactic nuclei (AGNs) into a semianalytic model of galaxy formation, adopting physically motivated scaling laws for accretion triggered by galaxy encounters. Our model reproduces the level of the cosmic X-ray background at 30 keV; we predict that the largest contribution (around two-thirds) comes from sources with intermediate X-ray luminosity $10^{43.5} < L_X/\mathrm{ergs\ s^{-1}} < 10^{44.5}$, with 50% of the total specific intensity produced at $z < 2$. The predicted number density of X-ray–luminous AGNs ($L_X > 10^{44.5}$ ergs s^{-1} in the 2–10 keV band) peaks at $z \approx 2$, with a decline of around 3 dex to $z = 0$; for the low-luminosity sources ($10^{43} < L_X/\mathrm{ergs\ s^{-1}} < 10^{44}$), it has a broader and less pronounced maximum around $z \approx 1.5$. The comparison with the data shows a generally good agreement. The model predictions slightly exceed the observed number of low-luminosity AGNs at $z \sim 1.5$, with the discrepancy progressively extending to intermediate-luminosity objects at higher redshifts; we discuss possible origins of the mismatch. Finally, we predict the source counts and the flux distribution at different redshifts in the hard (20–100 keV) X-ray band for the sources contributing to the X- ray background.

Subject headings: galaxies: active — galaxies: evolution — galaxies: formation — galaxies: interactions — X-rays: diffuse background — X-rays: galaxies

1. INTRODUCTION

The X-ray emission of active galactic nuclei (AGNs) provides a unique probe into the history of the accretion onto supermassive black holes (BHs) thought to power the AGNs. In fact, the X-rays probe the accretion down to BH masses as small as $m_{\mathrm{BH}} \sim 10^7\ M_\odot$ and to bolometric luminosities as low as $L \sim 10^{43}$ ergs s^{-1}. At redshifts of $z \gtrsim 0.5$, these regimes of accretion are hardly accessible to optical observations but may provide both a significant fraction of the total accretion power in the universe and a considerable contribution to the observed cosmic X-ray background (CXB).

At higher z, constraints on the properties of the AGNs, and hence on the history of accretion, have been derived by extrapolating local properties like the optical or X-ray luminosity functions or the X-ray spectral shape of nearby Seyfert galaxies. On the basis of these assumptions, several authors (see Madau, Ghisellini, & Fabian 1994; Comastri et al. 1995, 2001; Wilman & Fabian 1999) have constructed AGN synthesis models to account for the CXB; these authors argued that most of the accretion power producing the CXB at energies below 30 keV is intrinsically absorbed, as initially suggested by Setti & Woltjer (1989).

The drawbacks of such an approach are constituted by the degeneracies between different possible extrapolations and hence between synthesis models that still reproduce the observed integrated AGN properties. Furthermore, little direct insight can be gained on the physical links between the evolution of AGNs and that of their host galaxies. Until now, the incorporation of the X-ray properties of AGNs into a coherent picture of galaxy evolution is still lacking.

On the other hand, the attempt by Kauffmann & Haehnelt (2000) to connect the BH accretion to the evolution of galaxies in the hierarchical scenario was based on a semianalytic model (SAM) of galaxy formation of the kind introduced by Kauffmann, White, & Guiderdoni (1993) and Cole et al. (1994) and progressively developed by several authors (Somerville & Primack 1999; Wu, Fabian, & Nulsen 2000; Cole et al. 2000; Menci et al. 2002). Such a model assumed phenomenological and tunable scaling laws to connect the gas accreted onto the BH with the cold gas fraction available in the galaxies left over by the star formation. However, the model has been applied only to the bright quasar (QSO hereafter) population, yet it has failed to reproduce the fast drop (by a factor of $\sim 10^{-2}$) of their density observed from $z \approx 2$ to the present. A later paper by Nulsen & Fabian (2000) assumed that the BHs are specifically fueled by the cooling flows associated with the hot gas during the process of hierarchical galaxy evolution, the latter being described through a SAM. However, such a model fails to account for the observed relationship between the black hole and the spheroid masses (see Richstone et al. 1998); furthermore, it does not properly describe the statistical distribution of QSO properties in that it overpredicts their low-z luminosity functions and underpredicts QSOs at high z. Other analytic (see, e.g., Haiman & Loeb 1998; Wyithe & Loeb 2002; Hatziminaoglou et al. 2003), semianalytic (Volonteri, Hardt, & Madau 2003), or N-body (Kauffmann & Haehnelt 2002) works are based on major merging events of dark matter (DM) halos at high z as the only triggers for BH accretion, which is related to the DM mass of the halo either by adopting the locally observed relations or through phenomenological scaling laws; thus such models are suited to follow the QSO evolution at high-intermediate z but do not match the observed steep decline of the QSO density at redshifts of $z \lesssim 1$, a range of cosmic time of key interest for the activity of AGNs observed in X-rays.

Recently, Menci et al. (2003) developed a more physical model to connect BH accretion to galaxy evolution in the

[1] INAF-Osservatorio Astronomico di Roma, via di Frascati 33, I-00040 Monteporzio, Italy.
[2] Dipartimento di Fisica, Università di Roma Tre, via della Vasca Navale 84, I-00146 Rome, Italy.
[3] Dipartimento Fisica, II Università di Roma, via Ricerca Scientifica 1, I-00133 Rome, Italy.

hierarchical scenario. The accretion is triggered by galaxy encounters, not necessarily leading to bound merging, in common host structures such as clusters and especially groups; these events destabilize part of the galactic cold gas and hence feed the central BH, following the physical modeling developed by Cavaliere & Vittorini (2000, hereafter CV00). The amount of cold gas available, the interaction rates, and the properties of the host galaxies are derived through the SAM developed by Menci et al. (2002).

As a result, at high z the protogalaxies grow rapidly by hierarchical merging; meanwhile, much fresh gas is imported and also destabilized, so the BHs are fueled at their full Eddington rates. At lower z, the dominant dynamical events are galaxy encounters in hierarchically growing groups; now refueling peters out, as the residual gas is exhausted while the destabilizing encounters dwindle. With no parameter tuning other than that needed for star formation in canonical SAMs, the model naturally produces in the bright QSO population a rise for $z > 3$, and for $z \lesssim 2.5$ a drop as steep as observed. In addition, the results closely reproduce the observed luminosity functions of the optically selected QSOs, their space density at different magnitudes from $z \approx 5$ to $z \approx 0$, and the local $m_{\rm BH}$-σ relation.

Encouraged by the successes of the model, here we extend it to lower accretions and lower BH masses, in order to study the X-ray properties of the AGNs and to predict their contribution to the X-ray background. We avoid the introduction in our model of dust and gas obscuration, and therefore conservatively we compare our predicted CXB with the observations at energies $E \geq 30$ keV, the spectral region not affected by photoelectric absorption. At lower energies we compare our predicted number and luminosity densities of AGNs with data already corrected for dust and gas absorption.

The paper is organized as follows. In § 2 we recall the basic points of the galaxy evolutionary model upon which we base our work. The specific modeling that relates the BH accretion to the galaxy encounters is recalled in § 3, where we also describe how we obtain the X-ray luminosities. The results concerning the X-ray properties of AGNs at low and high z are compared with observations in § 4. Finally, § 5 is devoted to discussion and conclusions.

2. THE MODEL

2.1. *The Semianalytic Model of Galaxy Evolution*

The properties of the galaxies hosting the AGNs are derived using the SAM described in detail in Menci et al. (2003). Here we recall its basic points.

Following the procedure usually adopted in SAMs, we consider both the host DM halos (groups and clusters of galaxies with mass M, virial radius R, and circular velocity V) containing the galaxies and the DM clumps (with circular velocity v) associated with the individual member galaxies. The former grow hierarchically to larger sizes through repeated merging events (at the rate given, e.g., in Lacey & Cole 1993). On the other hand, the latter may coalesce either with the central galaxy in the common halo because of dynamical friction or with other companion galaxies through binary aggregations. We compute the probability of the latter processes occurring during the hierarchical growth of the host structure yields, at any cosmic time t, and the differential distribution $N(v, V, t)$ (per Mpc^3) of galaxies with given v in hosts with circular velocity V. From this we derive the number $N_T(V, t)$ of galaxies in a host halo (i.e., the membership) and the overall distribution of galaxy circular velocity $N(v, t)$, irrespective of the host halo. An average galaxy tidal radius $r_t(v)$ is associated with each galactic circular velocity v; the average relative velocity $V_r(V)$ of the galaxies in a common DM halo is computed for each circular velocity V of the host halo.

The properties of the gas and stars contained in the galactic DM clumps are computed as follows. Starting from an initial gas amount $m\,\Omega_b/\Omega$ ($m \propto v^3$ being the DM mass of the galaxies) at the virial temperature of the galactic halos, we compute the mass m_c of cold baryons residing in regions interior to the cooling radius. The disk associated with the cold baryons has radius $r_d(v)$ and rotation velocity $v_d(v)$, computed after Mo, Mao, & White (1998). From such a cold phase, stars are allowed to form with rate $\dot{m}_* = (m_c/t_d)(v/200\ \text{km s}^{-1})^{-\alpha_*}$, with the disk dynamical time evaluated as $t_d = r_d/v_d$.

Finally, a mass $\Delta m_h = \beta m_*$ is returned from the cool to the hot gas phase due to the energy fed back by canonical Type II supernovae associated with m_*. The feedback efficiency is taken to be $\beta = (v/v_h)^{\alpha_h}$; the values adopted for the free parameters $\alpha_* = -1.5$, $\alpha_h = 2$, and $v_h = 150$ km s^{-1} fit both the local B-band galaxy luminosity function and the Tully-Fisher relation, as illustrated by Menci et al. (2002). The model also matches the bright end of the galaxy B-band luminosity functions up to redshifts of $z \approx 3$ (see Poli et al. 2003), and the resulting global star formation history is broadly consistent with that observed up to a redshift of $z \approx 4$ (Fontana et al. 1999).

At each merging event, the masses of the different baryonic phases are replenished by those in the merging partner; the further increments Δm_c, Δm_*, and Δm_h from cooling, star formation, and feedback are recomputed upon iterating the procedure described above.

Thus, for each galactic circular velocity the star formation described above is driven by the cooling rate of the hot gas and by the rate of replenishing of the cold gas, which in turn is related to the progressive growth of the total galactic mass along the galaxy merging tree. The integrated stellar emission $S_\lambda(v, t)$ at the wavelength λ is computed by convolving the star formation rate with the spectral energy distribution ϕ_λ obtained from population synthesis models (Bruzual & Charlot 1993 and subsequent updates).

All computations are made in a ΛCDM cosmology with $\Omega_0 = 0.3$, $\Omega_\lambda = 0.7$, a baryon fraction $\Omega_b = 0.03$, and a Hubble constant $h = 0.7$ in units of 100 km s^{-1} Mpc^{-1}.

2.2. *Accretion onto Supermassive BHs*

We follow the model presented in Menci et al. (2003) to derive the fraction of the galactic cold gas accreted onto the central BH. Galaxy encounters are expected to destabilize part of such gas, causing it to loose angular momentum (Mihos & Hernquist 1996; Barnes & Hernquist 1998; see also Mihos 1999) and thus triggering gas inflow.

The fraction of cold gas destabilized in each interaction event is computed in equation (A3) of CV00 in terms of the variation Δj of the specific angular momentum $j \approx Gm/v_d$ of the gas, to read

$$f(v, V) \approx \frac{1}{8}\left|\frac{\Delta j}{j}\right| = \frac{1}{8}\left\langle \frac{m'}{m}\frac{r_d}{b}\frac{v_d}{V}\right\rangle. \quad (1)$$

Here $b = \max\,[r_d, R/N_T^{-1/3}(V)]$ is the impact parameter, m' is the mass of the partner galaxy in the interaction, and the

average runs over the probability of finding a galaxy with mass m' in the same halo V where the galaxy m is located. The prefactor accounts for the probability (1/2) of inflow rather than outflow related to the sign of Δj. In addition, the gas funneled inward may end up also in a nuclear starburst; the relative amount has been estimated from 3/1 to 9/1 (see Sanders & Mirabel 1996; Franceschini, Braito, & Fadda 2002). Here we assume that one-fourth of the inflow feeds the central BH, while the remaining fraction kindles circumnuclear starbursts, tackled in detail by Menci et al. (2004).

The rate of nearly grazing encounters for a galactic halo with given v inside a host halo (group or cluster) with circular velocity V is given by $\tau_r^{-1} = n_T(V)\Sigma(v, V)V_r(V)$; here $n_T = N_T/(4\pi R^3/3)$, and the cross section $\Sigma(v, V) \approx \pi\langle(r_t^2 + r_t'^2)\rangle$ is averaged over all partners with tidal radius r_t' in the same halo V. The membership N_T and the distributions of v', r_t', and V_r are computed from the SAM as described in § 2.

The average gas accretion rate triggered by interactions at z is given by (see eq. [5] of CV00 and Menci et al. 2003)

$$\dot{m}_{\rm acc}(v, z) = \left\langle \frac{f(v, V)m_c(v)}{\tau_r(v, V)} \right\rangle, \quad (2)$$

where the average is over all host halos with circular velocity V. The mass of the BH hosted in a galaxy with given v at time t is updated after $m_{\rm BH}(v, t) = (1 - \eta)\int_0^t \dot{m}_{\rm acc}(v, t')dt'$, where $\eta \approx 0.1$ (see Yu & Tremaine 2002) is the mass-energy conversion efficiency; here we assume in all galaxies initial seed BHs of mass much smaller than the active supermassive BHs (see Madau & Rees 2001).

The bolometric luminosity so produced by the accretion onto a BH hosted in a galaxy with given v then reads

$$L(v, t) = \frac{\eta c^2 \Delta m_{\rm acc}}{\tau}. \quad (3)$$

Here $\tau \approx t_d \sim 5 \times 10^7 (t/t_0)$ yr is the duration of the accretion episode, i.e., the timescale for the QSO to shine; $\Delta m_{\rm acc}$ is the gas accreted at the rate given by equation (2). The blue luminosity L_B is obtained by applying a bolometric correction of 13 (Elvis et al. 1994), while for the unabsorbed X-ray luminosity L_X (2–10 keV) we adopt a bolometric correction $c_{2-10} = 100$ following Elvis, Risaliti, & Zamorani (2002); for simplicity, this is assumed to be constant with z. The shape of the X-ray spectrum $I(E)$ is assumed to be a power law with a slope $\alpha = 0.9$ (see Comastri 2000 and references therein), with an exponential cutoff at an energy $E_c = 300$ keV (see, e.g., Perola et al. 2002 and references therein); in view of the present data situation we keep this as our fiducial shape. The effect of the scatter in α and E_c will be discussed in § 4.

The evolving luminosity function is derived from $N(v, t)$ by applying the appropriate Jacobian given by equation (3) with the appropriate bolometric correction. The luminosity function will include a factor $\tau/\langle\tau_r(v)\rangle < 1$ since the luminosities in equation (3) last for a time τ and are rekindled after an average time τ_r. The result is

$$N(L, t) = N(v, t)\frac{\tau}{\langle\tau_r\rangle}\left|\frac{dv}{dL}\right|. \quad (4)$$

As shown by Menci et al. (2003), the model produces a drop of the bright ($M_B < -24$) QSOs as steep as observed. This results from the combined decrease with time of both the interaction rate τ_r^{-1} and the accreted fraction f (see Fig. 1 in Menci et al. 2003). These in turn are caused by the decrease of the encounter probability due to the decrease of the number density of galaxies inside the host groups/clusters and to the simultaneous increase of galaxy relative velocities V_r. For massive galaxies, the above effects also combine with the decrease of the available amount of cold gas, due to its rapid conversion into stars in the early phases of star formation.

The above effects concur and produce number densities and luminosity functions of QSOs in excellent agreement with the observations in the full range $0 < z < 6$, as shown in Menci et al. (2003). But comparison with optical data allows us to probe the model only in the medium-high accretion regimes, corresponding to optical magnitudes brighter than $M_B \approx -24$. Here we explore the predictions of our model down to accretion rates lower by a factor of $\sim 10^{-1}$, which at present can only be probed by X-rays.

3. THE OVERALL PICTURE

Before presenting in detail our results and comparing them with observations, we give an overview of the picture concerning the BH accretion in evolving galaxies as it emerges from our model. In Figure 1 we show the volume emissivity from the AGNs that at redshift z have luminosity L_X. Since our model links the evolution of AGNs to that of hierarchically growing galaxies, we can gain some insight also on the hosts of the AGNs contributing to the accretion history of the universe. So we also show in the figure the evolutionary tracks of AGNs hosted in galaxies with different masses.

At redshifts from 6 to 3, a rapid increase in the accretion is sustained by the continuous replenishing of cold gas due to the frequent galaxy merging events and to the high rate of encounters that destabilize it. The trade-off between high luminosity and large number of sources determines a peak in the global emissivity at intermediate AGN luminosities $L_X \sim 10^{44}$ ergs s^{-1}, which are hosted typically in galaxies with DM mass of 5×10^{10} to 3×10^{11} $M_\odot$.

At later z the era of galaxy formation ends, the merging rate of galaxies drops, and the cold gas replenishing dwindles. The encounter rate of galaxies also decreases, and the galaxies enter a era of nearly passive evolution. The AGNs in the most massive galaxies (with DM masses of $M > 10^{12}$ $M_\odot$) show the most dramatic decrease in luminosity (Fig. 1, *leftmost track*), since their host galaxies have already converted most of their gas into stars at higher z. The decrease at $z \lesssim 1.8$ of the luminosities of the AGN population produces the decrease in the total emissivity shown in Figure 1.

The location of the peak in both redshift and luminosity, as well as the specific evolution with z of the luminosity of AGNs hosted in galaxies with different masses, strongly affects the relative contribution of different classes of AGNs to the CXB and the redshift distribution of their number or luminosity density, as we show in detail below.

4. RESULTS

We compute the contribution to the CXB from the luminosity functions in equation (4) as follows:

$$\frac{d^2F(E)}{dE\,d\omega} = \int dV \int_{L_1}^{L_2} dL_X N(L_X, z)\frac{I[L_X, E(1+z)]}{4\pi d_L^2}. \quad (5)$$

Here dV is the cosmic volume element per unit solid angle ω, d_L is the luminosity distance, and $I(L, E)$ is the AGN spectrum.

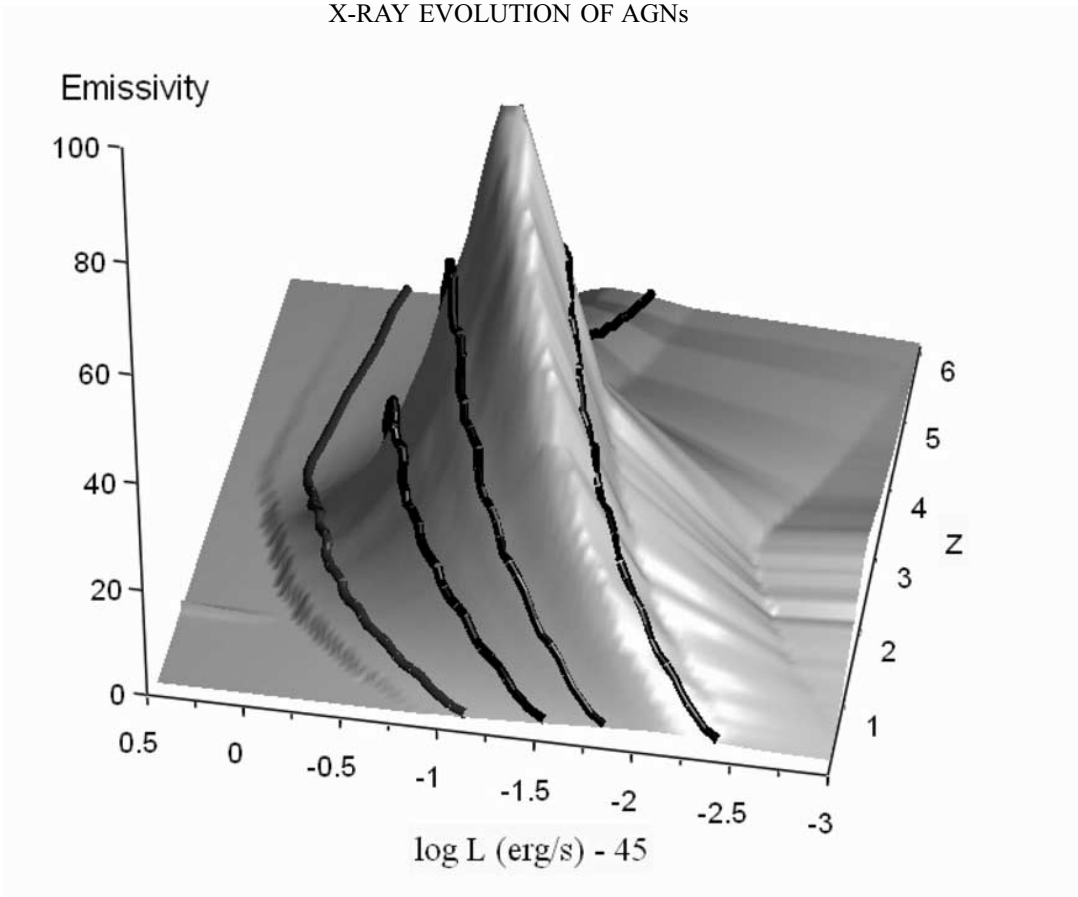

FIG. 1.—Overall X-ray emissivity contributed by AGNs with given X-ray luminosity L_X and redshift z. We also show the evolutionary tracks of the luminosity of AGNs hosted in galaxies with different DM masses corresponding to (*from left to right*) 10^{13}, 10^{12}, 2.5×10^{11}, and 5×10^{10} $M_\odot$.

This is normalized to yield $L_X = L/c_{2-10}$ when integrated in the rest-frame energy range 2–10 keV. We consider the contribution to the CXB from AGNs in specific luminosity ranges $\Delta L = [L_1, L_2]$. The total CXB is obtained upon integrating over the full range of luminosities $10^{42} < L_X/\mathrm{ergs\ s^{-1}} < 5\times10^{46}$ spanned by our SAM.

Since the model does not include obscuration, we directly compare the results from equation (5) with the hard CXB observed at $E \geq 30$ keV, where photoelectric absorption does not affect the observed fluxes. Nonetheless, we must be aware of the fact that even at this energy, the value of the observed background is appreciably affected by the presence of sources in a Compton-thick phase of obscuration.

In Figure 2 we show the hard CXB at $E_0 = 30$ keV obtained from equation (5) by integrating the volume out to running redshift z. We show both the global value and the fraction contributed by AGNs in three classes of luminosity. The predicted background with the chosen parameters for the spectrum ($\alpha = 0.9$, $E_c = 300$ keV, and $c_{2-10} = 100$; see § 2.2) exceeds the value measured by *HEAO 1* A-2 by no more than 50%.

At the present state of our observational knowledge, the substantial agreement is very encouraging, especially if the following points are taken into account: (1) the available evidence (at $E < 10$ keV; Lumb et al. 2002; Vecchi et al. 1999) that the CXB normalization from the *HEAO 1* A-2 experiment may be underestimated by as much as 30%, (2) the bolometric correction needs to take on the fixed value that we adopted for all values of L and L/L_{Edd}, and (3) the incidence of a Compton-thick phase along the active phase of a galactic nucleus, as a function of L and z, is not known, except that locally it may amount as much as 50% (Risaliti, Maiolino, & Salvati 1999) of the so-called type 2 AGNs, namely those with

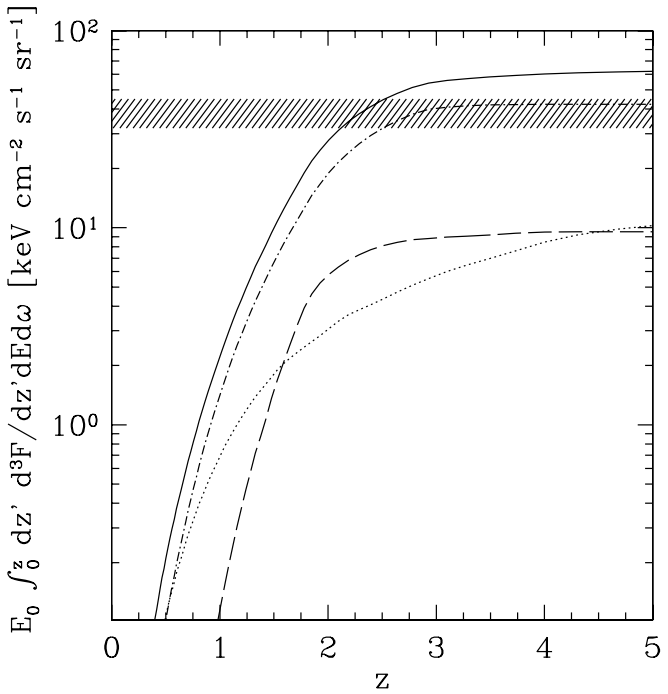

FIG. 2.—Cumulative contribution (multiplied by the energy E_0) to the predicted CXB at $E_0 = 30$ keV, yielded by sources at progressively larger redshifts. The solid line shows the total CXB produced by sources with all luminosities. The other lines show the contributions of AGNs with luminosities L_X (in units of ergs s^{-1}, in the band 2–10 keV) in the ranges $42 < \log L_X < 43.5$ (*dotted line*), $43.5 < \log L_X < 44.5$ (*dot-dashed line*), and $44.5 < \log L_X$ (*long-dashed line*). The shaded strip is the value 43 keV cm^{-2} s^{-1} sr^{-1} measured by *HEAO 1* A-2 (Gruber et al. 1999).

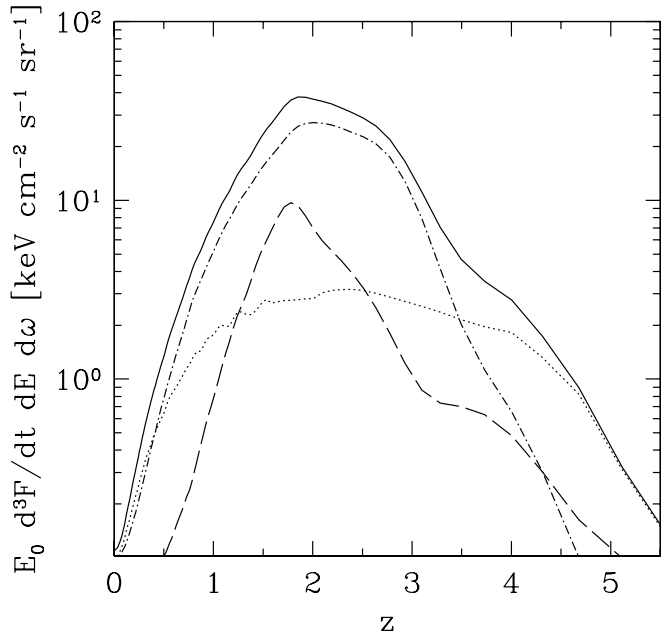

FIG. 3.—Differential contribution to the predicted CXB at $E_0 = 30$ keV, for different ranges of luminosity of the contributing sources. Symbols are as in Fig. 2.

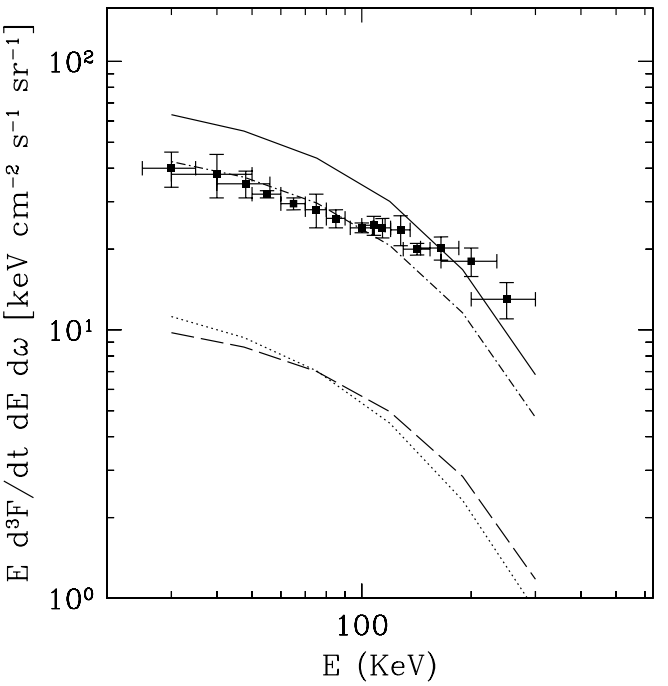

FIG. 4.—Energy spectrum of the predicted CXB for $E \geq 30$ keV, for different ranges of luminosity of the contributing sources. Symbols are as in Fig. 1. Data are from Gruber et al. (1999).

a substantial obscuration both in the optical as well as in the X-ray band. The essential features of our predictions are shown in Figures 2 and 3.

Figure 2 shows that in our model the CXB is mainly contributed by AGNs with intermediate luminosities $L_X = 10^{43.5}$–$10^{44.5}$ ergs s^{-1}, which provide ≈50% of the total value. High-luminosity ($L_X > 10^{44.5}$ ergs s^{-1}) and low-luminosity ($L_X < 10^{43}$ ergs s^{-1}) sources contribute a fraction of ∼25% each. The population with intermediate luminosities strikes the best trade-off between larger luminosity and smaller number of sources. Thus, in this picture high-luminosity, highly absorbed objects (the so-called type 2 QSOs) would not give a dominant contribution to the hard CXB. In fact, although recent *XMM* and *Chandra* surveys are providing a sizeable number of QSO 2s (Barger et al. 2002; Fiore et al. 2003; Hasinger 2003), these are likely to constitute a relatively minor fraction of sources down to the fluxes where the bulk of the hard CXB is resolved into sources.

Note also that while the contribution of the high-luminosity sources saturates already at $z \approx 2$, that from low-luminosity ones continues to rise up to $z \approx 3-4$. This behavior can be regarded as a natural outcome in the framework of a hierarchical scenario, where at earlier times increasingly larger numbers of small galaxies are present, which later merge to form larger systems.

Further insight into the redshift distribution of the contribution to the CXB at 30 keV is provided in Figure 3, which shows the z-derivative of the CXB in Figure 2. The contribution of all sources to the CXB peaks at $z \approx 2$, and so does the contribution of the intermediate-luminosity sources. The contribution of high-luminosity AGNs, instead, is more sharply peaked at the slightly lower redshift, $z \approx 1.7$, while the contribution of the lowest luminosity sources shows a broad z-distribution.

The CXB spectrum above 20 keV, computed with the fixed values of α and E_c given above, is compared with the *HEAO 1* A-2 data in Figure 4. Apart from the normalization mismatch commented on previously, the predicted shape is slightly softer than observed. We note however that in a more detailed modeling, the adoption of an appropriate scatter in α and E_c is likely to yield a somewhat harder shape.

Our model can provide guidelines for future observations. Figure 5 shows the differential (*top*) and integral (*bottom*) contribution to the CXB at various energies (from 30 to

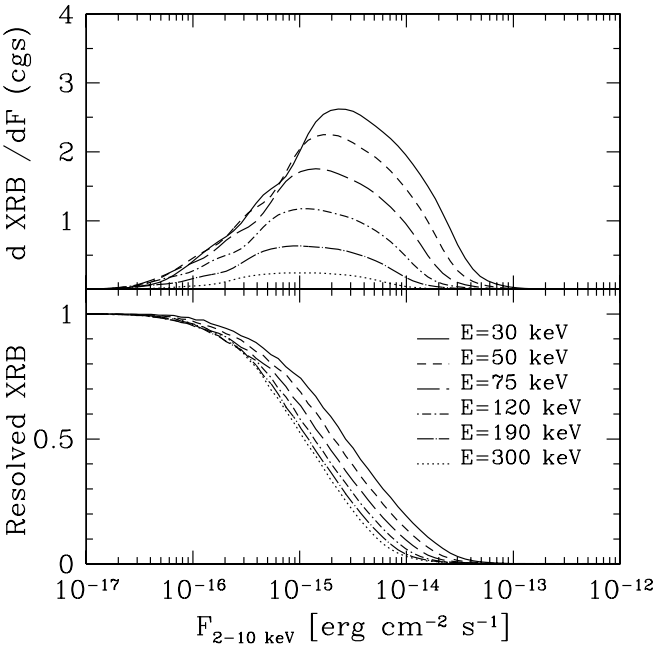

FIG. 5.—*Top*: Flux distribution of AGNs contributing to the CXB at different energies (see labels in the bottom panel). The flux corresponds to the intrinsic emission (corrected for obscuration) in the currently accessible energy band 2–10 keV. *Bottom*: Fraction of the CXB contributed by sources with fluxes larger than the considered value.

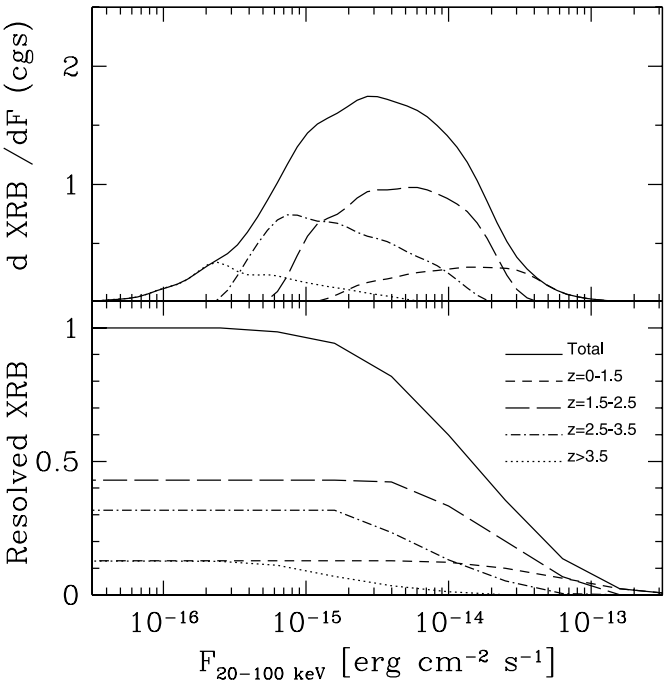

FIG. 6.—*Top*: 20–100 keV flux distribution of AGNs contributing to the CXB at 30 keV for different bins of redshift (see labels in the bottom panel). *Bottom*: Fraction of the CXB contributed by sources brighter than the value in abscissa, for the different redshift shells.

300 keV) provided by sources with different 2–10 keV flux (corrected for obscuration). As a function instead of their 20–100 keV flux, the panels in Figure 6 show the differential and the integral contributions to the CXB at 30 keV in various bins of redshifts, from $z = 0-1.5$ to $z > 3.5$. This figure illustrates the predictions that the bulk of the CXB should be provided by sources with fluxes of around $F_{20-100\,\mathrm{keV}} \approx 10^{-14}$ ergs cm^{-2} s^{-1}, placed at redshifts of $z \approx 1.5-2.5$. To observationally access this flux level, high energy focusing optics are required, a technological step forward that has become feasible and is included in current studies for further missions, e.g., Constellation-X [4] and NeXT (Tawara et al. 2003).

Figure 7 shows the source counts expected in our model in the 13–80 keV band, to be compared with the *HEAO 1* A-4 data point (Levine et al. 1984); note that the predicted counts agree very well with the bright flux point. We also compare our predictions with the extrapolation to the 13–80 keV band of the *BeppoSAX* HELLAS 5–10 keV counts, assuming spectral shapes depending on different values of the adopted absorbing columns. This comparison suggests that the bulk of the hard X-ray selected sources with flux at a few 10^{-13} ergs cm^{-2} s^{-1} has a substantial absorbing column, of the order of $N_{\mathrm{H}} = 10^{23}$ cm^{-2}.

So far we have compared the predictions of our model with integrated observations, i.e., the spectrum of the CXB at energies higher than 30 keV and the hard X-ray counts. We now proceed to compare the model with observations of differential nature in redshift and in luminosity, which can provide tighter constraints. Here the comparison is more critical because of the difficulty of obtaining well-defined, complete samples of highly obscured AGNs at redshifts of $z \approx 2.5-3$. The most recent results on the number and luminosity density of AGNs come from *Chandra* and *XMM-Newton* deep pencil beam surveys: the North and South Chandra Deep Fields (Brandt et al. 2002; Barger et al. 2002; Giacconi et al. 2002; Cowie et al. 2003) and the Lockman Hole survey (Hasinger 2003). We compare with the wider but shallower surveys from *XMM-Newton* (Fiore et al. 2003). In particular, the latter authors combined the results of the optical identification of the HELLAS2XMM 1dF survey with carefully selected identifications from deep *Chandra* and *XMM* surveys to obtain a well-defined, flux-limited sample of 317 hard X-ray selected sources (2–10 keV), 70% of them with a measured redshift. These observations were performed in the 2–10 keV band; hence they imply generally small uncertainties affecting the correction for line-of-sight obscuration in the derivation of rest-frame luminosity.

In Figure 8 we compare our predictions with the evolution of the number and luminosity densities of AGNs in three luminosity bins, estimated by Fiore et al. (2003). Note that the three luminosity bins adopted by Fiore et al. (2003) for statistical reasons differ from those adopted in Figure 2, which were chosen to single out the class of objects producing the dominant contribution to the CXB.

All the predicted densities drop substantially from $z \approx 2$ to the present. The agreement with the data is excellent for the highest luminosity bin, which is not surprising since such objects are also sampled in the optical band, where the model was already successfully tested in Menci et al. (2003). In addition, Fiore et al. (2003) find a nice agreement between their data for high-luminosity sources and the evolution of optically selected AGNs with $M_B < -24$ estimated by Hartwick & Shade (1990). This agreement confirms that, at least for the very luminous AGNs, the bolometric corrections adopted in the B and in the X-ray band are fully consistent.

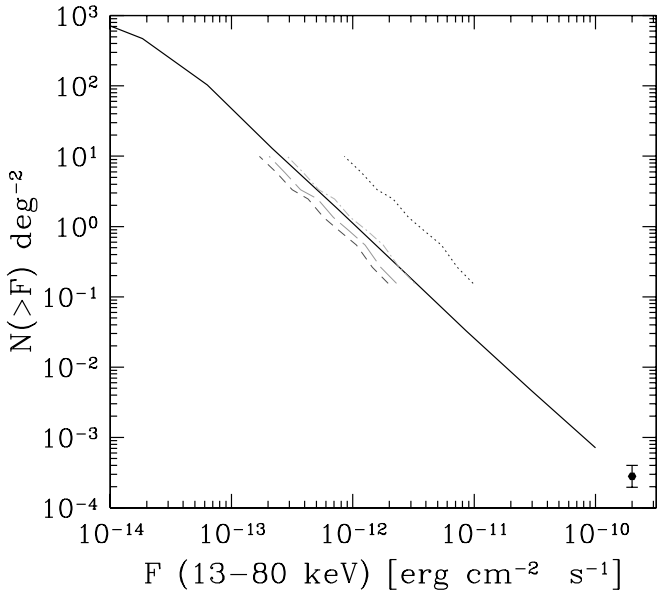

FIG. 7.—Source counts of hard X-ray AGNs contributing to the CXB shown for the band 13–80 keV and compared with the *HEAO 1* A-4 data point (Levine et al. 1984). We also show the extrapolation to the 13–80 keV band of the *BeppoSAX* HELLAS 5–10 keV counts on assuming different absorbing column densities: $N_{\mathrm{H}} = 10^{21}$ cm^{-2} (*short-dashed line*), 10^{23} cm^{-2} (*long-dashed line*), $10^{23.5}$ cm^{-2} (*dot-dashed line*), and 10^{24} cm^{-2} (*dotted line*).

[4] See http://constellation.gsfc.nasa.gov.

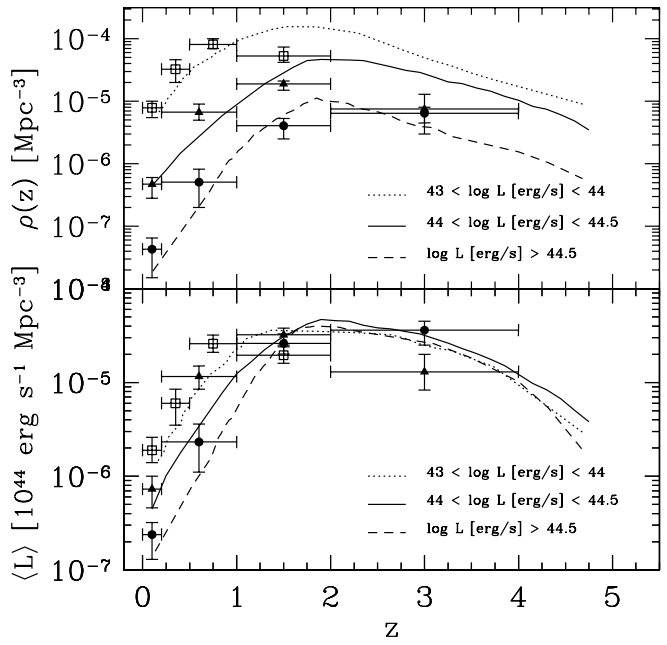

FIG. 8.—*Top*: Evolution of the number density of X-ray AGNs in three bins of luminosity (in units of ergs s^{-1}, in the band 2–10 keV): $43 < \log L_X < 44$ (*dotted line*), $44 < \log L_X < 44.5$ (*solid line*), and $44.5 < \log L_X$ (*dashed line*). The data for the above luminosity bins (*squares, triangles, and circles, respectively*) are taken from Fiore et al. (2003). *Bottom*: Evolution of the X-ray luminosity density for the same luminosity bins.

At lower luminosities, the decline for $z < 1-2$ is less pronounced in the predictions, as well as in the observations. In the former, this is due to the larger quantity of galactic cold gas left available for accretion in the less massive galaxies. This is a natural feature in hierarchical scenarios, since more massive potential wells originate from clumps collapsed earlier in *biased* regions of the primordial perturbation field; the higher densities then prevailing allowed for earlier condensation and hence enhanced star formation at high redshifts. Thus, at low z a larger fraction of cold gas will have already been converted into stars, and both star formation and BH accretion are considerably suppressed. We note though that the decrease of the peak redshift with decreasing luminosity appears to be significantly smaller than indicated by the data. In particular, at $z = 1$–2 the observed density of Seyfert-like AGNs is a factor $\approx$2 lower than predicted by the model; a similar difference is present also for the intermediate-luminosity objects ($L_X = 10^{44}-10^{44.5}$ ergs s^{-1}) in the redshift bin $z = 2$–4.

The reason for such a discrepancy can be traced back to the shape of the high-z X-ray luminosity function. This is shown in Figure 9, where we compare our model results with the observational luminosity functions derived by Fiore et al. (2003; *top*) and by Ueda et al. (2003; *bottom*), which are obtained from a combination of *HEAO 1*, *ASCA*, and *Chandra* data and extend down to lower luminosities. The above observational results concur and indicate that the luminosity functions at $z \gtrsim 2$ are appreciably flatter than at $z = 0.5$–1. When the above data are compared with our results, a substantial agreement is found at low z, while at $z \gtrsim 1.5$–2 the model overestimates the number of low-luminosity objects found in both the observational analyses. Such a mismatch cannot be reduced by fine-tuning the bolometric correction c_{2-10} adopted in our model, since the latter affects only the normalization of the luminosities.

5. DISCUSSION

We have incorporated the description of the X-ray properties of AGNs into the hierarchical picture of galaxy evolution. Our SAM, already proven to match the observed evolution of luminous optically selected QSOs over the redshift range $0 < z < 6$ (Menci et al. 2003), is here extended to bolometric luminosities L a factor of 10 lower. So we describe the history of accretion down to $L \sim 10^{45}$ ergs s^{-1}, for which the main observational information comes from the X-ray band.

We have compared our model with X-ray observations either corrected for gas obscuration or performed in the hard ($E > 30$ keV) band not affected by photoelectric absorption. We find that our model is encouragingly able to match the level of the CXB at 30 keV (Fig. 2). We predict that the largest contribution (around two-thirds) to the CXB comes from intermediate-luminosity sources of $43.5 < \log (L_X/\text{ergs s}^{-1}) < 44.5$ and that 50% of its total specific intensity is produced at $z < 2$ (see Figs. 2 and 3). The predicted 30–300 keV CXB spectrum shown in Figure 3 has been computed with the simplifying assumption of a fixed spectrum for all individual sources and neglecting the absorption in Compton-thick sources. If a spread in the spectral slope α and in the high-energy cutoff E_c is included, a harder spectrum would

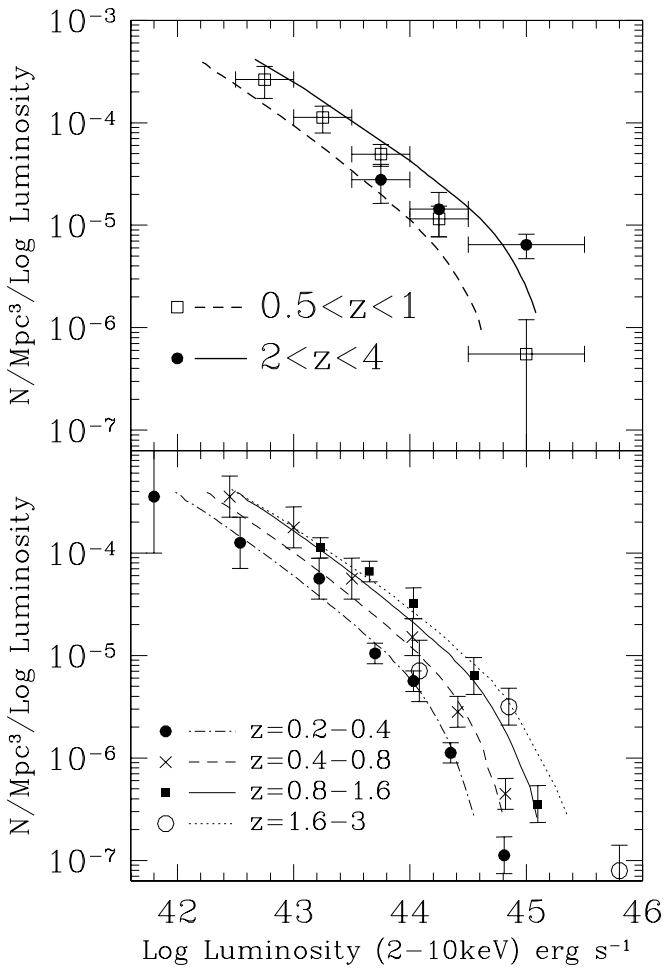

FIG. 9.—*Top*: Predicted luminosity functions in the energy range 2–10 keV at low redshifts $0.5 < z < 1$ (*dashed line*) and high redshifts $2 < z < 4$ (*solid line*) compared with observational values derived from the same sample used in Fiore et al. (2003) to derive the densities in Fig. 8. *Bottom*: Predicted luminosity functions in the energy range 2–10 keV compared with the observational values obtained by Ueda et al. (2003) at various redshifts.

naturally obtain. Concurrently, if the distribution of Compton-thick sources is skewed toward larger redshifts, the absorption would not affect the spectrum at large energies ($E \gtrsim 100$ keV), where the CXB is contributed mainly by low-redshifts sources; this results in an effective flattening of the spectrum. Since the inclusion of both these effects in the model would lead to a harder spectrum, a confirmation of the slope measured by *HEAO 1* A-4 with future experiments would be of major interest.

We also predict (Figs. 6 and 7) the number counts and the flux distribution at different z in the hard (20–100 keV) X-ray band for the sources contributing to the X-ray background. We have shown that ~50% of the CXB at 30 keV is produced by sources brighter than 2×10^{-14} ergs cm^{-2} s^{-1} in the 20–100 keV band. Such predictions can provide guidelines for aimed observations and future experiments.

When compared with the observed evolution of the number and luminosity densities of AGNs with different L_X (Fig. 8), our model agrees with the observations concerning all luminosities $L_X > 10^{43}$ ergs s^{-1} for low or intermediate redshifts $z \lesssim 1.5-2$. Thus, adopting a universal spectrum (and hence fixed bolometric corrections), our model matches the observations concerning both the optical (see Menci et al. 2003) and the X-ray bands, at least for objects with bolometric luminosities $L \gtrsim 10^{46}$ ergs s^{-1}; in particular, the density of luminous ($L_X > 10^{44.5}$ ergs s^{-1}) AGNs peaks at $z \approx 2$, while for the low-luminosity sources ($10^{43} < L_X/\text{ergs s}^{-1} < 10^{44}$) it has a broader maximum around $z \approx 1.5$; the decline from the maximum to the value at the present epoch is around 3 dex for the former class and 1.5 dex for the latter class. At larger redshifts $z \gtrsim 2$, the model still reproduces the observed number and luminosity densities of AGNs stronger than $10^{44.5}$ ergs s^{-1}, but at $z = 1-2$ the predicted density of Seyfert-like AGNs is a factor of ≈2 larger than observed; a similar difference is present also for the intermediate-luminosity objects ($L_X = 10^{44}-10^{44.5}$ ergs s^{-1}) in the redshift bin $z = 2-4$. We next discuss our interpretation of both the low-z and the high-z results.

For $z \lesssim 2$, the model results agree with the observed number and luminosity densities in indicating a drop of the AGN population for $z < 2$ that is faster for the strongest sources. In our picture the drop is due to the combined effects of (1) the decrease of the galaxy merging and encounter rates, which triggers the gas destabilization and the BH feeding in each galaxy, and (2) the decrease of the galactic cold gas, which was already converted into stars or accreted onto the BH. The faster decline that obtains in massive galaxies (and hence for luminous AGNs) is related in particular to the latter effect. Indeed, in hierarchical clustering scenarios the star formation history of larger objects peaks at higher z, since massive objects originate from progenitors collapsed in biased regions of the universe where/when the higher densities allowed for earlier star formation; so at low z, such objects have already exhausted most of their gas. On the other hand, less massive galaxies are continuously enriched by low-mass satellites, whose star formation is more smoothly distributed in z and which retain even at $z \approx 0$ an appreciable fraction of cold gas available for BH accretion.

For $z \gtrsim 2$, the slight excess of the number and luminosity densities of weak AGNs with $L_X < 10^{44.5}$ ergs s^{-1} over the observations may originate both in the observations and in the modeling. On one hand, data incompleteness is to be expected at high z for low-luminosity objects. Although the data are corrected for absorption, the sources would be lost from the sample when heavily obscured below the detection limit. Also, the observed number and luminosity densities do not include Compton-thick sources, whose contributions are included in the model predictions. If the amount of obscuring gas increased with redshift, as would be the case if a large amount of gas accumulates in the surroundings of Eddington-limited BHs, sources with lower z and higher luminosity would be effectively favored. Future observations extended to harder bands will clarify the issue; in the meantime, we plan to improve the comparison between the model and the data through the inclusion in the model of gas absorption and the computation of the related effect of Compton-thick sources. This in principle can be done self-consistently, since the amount of galactic gas is predicted in our model (see Fig. 1 in Menci et al. 2003).

On the other hand, the excess of predicted low-luminosity AGNs at high z could originate from an incomplete modeling in the low-mass regime at high z. For example, the mismatch may be lifted by a mean AGN lifetime increasing with mass (see Yu & Tremaine 2002), a feature that can be implemented in the developments of our present fiducial model, specifically through a mass dependence of τ in equations (3) and (4). Additional improvements may concern the following factors:

1. *The properties of the accretion disks at low accretion rates*.—Advection-dominated accretion flows might constitute an example of such physics, although they ought to decrease the emitted luminosity preferentially at high z to explain the excess.

2. *The regulations governing the amount of cool gas in low-mass host galaxies, such as supernovae feedback*.—This still represents the most uncertain factor of all SAMs; it is known to play a key role in flattening the faint end of the optical galaxy luminosity functions, since large feedback would deplete the cold gas reservoirs preferentially in shallow potential wells.

3. *The statistics of DM halos*.—The most recent N-body simulations point toward a mass function of galactic DM clumps somewhat flatter at the small-mass end than previously assumed (see Sheth & Tormen 1999; Jenkins et al. 2001). While this could contribute to solving the issue, the flattening is not large enough to explain the observed excess.

All the above points can concur in determining the excess of the predicted low-luminosity AGNs at high z. We note, however, that overprediction of the low-luminosity sources is a long-standing problem that also affects the number and luminosity distribution of faint, high-z galaxies. This would point toward an origin of the mismatch in the physics of galaxy formation rather than in the description of the accretion processes. If this is indeed the case, tuning the free parameters in the SAM (such as, e.g., the efficiency of supernovae feedback, the main one that suppresses the AGN and star formation activity in low-mass systems) does not constitute a valid solution for the excess of low-luminosity X-ray AGNs at high z; in fact, the required adjustments would worsen the matching between the model results and the observed properties of galaxies, such as, e.g., the Tully-Fisher relation. On the other hand, implementing an ad hoc parametrical dependence on z of supernovae feedback could significantly reduce the excess, but in the absence of a physical motivation, this would not lead to a deeper insight into the galaxy-AGN connection.

Thus, a real improvement in the modeling requires the inclusion of additional physical processes in the SAM (and in particular in the factor concerning the feedback), rather than the tuning of the parameters in the existing framework. One such process could be well constituted by the inclusion into

SAMs of the feedback produced by the AGN emission itself. Since the AGN activity strongly increases with redshift, this could significantly contribute to expelling/reheating part of the galactic cold gas reservoir in low-mass systems at high z. While the modeling of such impulsive processes is particularly delicate, some steps in this direction have already been taken (see, e.g., Haehnelt, Natarajan, & Rees 1998; Silk & Rees 1998; Wyithe & Loeb 2003; Cavaliere, Lapi, & Menci 2002 and references therein). We shall investigate the effects of such processes on the evolution of the AGN population in our next paper.

In sum, despite the uncertain origin of the overprediction of faint X-ray sources at $z \gtrsim 2$, the present model provides a good baseline for including the evolution of galaxies and AGNs in the same global picture, being supported by a remarkable agreement with the observations of its predictions for brighter sources in a wide range of redshifts (from $0 < z < 6$) and of wavelengths (from optical to X-rays). The most distinctive feature of such a picture is the dramatic decrease of the AGN luminosities at $z \lesssim 2$, especially in massive galaxies (see Fig. 1), naturally resulting from the exhaustion of cold gas necessary for feeding both the accretion and the star formation; in a related manner, massive galaxies are predicted to undergo a nearly passive evolution from $z \approx 2$ to the present. The relevance of such an exhaustion in determining the observed properties of the AGN population (in both the optical and the X-rays) is confirmed by recent N-body simulations (Di Matteo et al. 2003). The above picture thus naturally explains the parallel evolution of BH accretion and star formation in spheroidal systems; this, originally discussed by Monaco, Salucci, & Danese (2000) and Granato et al. (2001), is supported by recent works (see Franceschini et al. 1999; Haiman, Ciotti, & Ostriker 2004), which also enlighten us on its simultaneous consistence with the evolution of the optical and the X-ray luminosity functions of AGNs (Cattaneo & Bernardi 2003). The physical origin of such a parallel evolution is here clarified and shown to arise as a natural outcome of hierarchical galaxy formation.

REFERENCES

Barger, A., Cowie, L., Brandt, W. N., Capak, P., Garnire, G. P., Hornschemeier, A. E., Steffen, A. T., & Wehner, E. H. 2002, AJ, 124, 1839
Barnes, J. E., & Hernquist, L. E. 1998, ApJ, 495, 187
Brandt, W. N., et al. 2002, ApJ, 569, L5
Bruzual A., G., & Charlot, S. 1993, ApJ, 405, 538
Cattaneo, A., & Bernardi, M. 2003, MNRAS, 344, 45
Cavaliere, A., Lapi, A., & Menci, N. 2002, ApJ, 581, L1
Cavaliere, A., & Vittorini, V. 2000, ApJ, 543, 599 (CV00)
Cole, S., Aragón-Salamanca, A., Frenk, C. S., Navarro, J. F., & Zepf, S. E. 1994, MNRAS, 271, 781
Cole, S., Lacey, C. G., Baugh, C. M., & Frenk, C. S. 2000, MNRAS, 319, 168
Comastri, A. 2000, in AIP Conf. Proc. 599, X-Ray Astronomy: Stellar Endpoints, AGN, and the Diffuse X-Ray Background, ed. N. White, G. Malaguti, & G. G. C. Palumbo (Melville: AIP), 73
Comastri, A., Fiore, F., Vignali, C., Matt, G., Perola, G. C., & La Franca, F. 2001, MNRAS, 327, 781
Comastri, A., Setti, G., Zamorani, G., & Hasinger, G. 1995, A&A, 296, 1
Cowie, L. L., Barger, A. J., Bautz, M. W., Brandt, W. N., & Garmire, G. P. 2003, ApJ, 584, L57
Di Matteo, T., Croft, R. A. C., Springel, V., & Hernquist, L. 2003, ApJ, 593, 56
Elvis, M., Risaliti, G., & Zamorani, G. 2002, ApJ, 565, L75
Elvis, M., et al. 1994, ApJS, 95, 1
Fiore, F., et al. 2003, A&A, 409, 79
Fontana, A., Menci, N., D'Odorico, S., Giallongo, E., Poli, F., Cristiani, S., Moorwood, A., & Saracco, P. 1999, MNRAS, 310, L27
Franceschini, A., Braito, V., & Fadda, D. 2002, MNRAS, 335, L51
Franceschini, A., Hasinger, G., Miyaji, T., & Malquori, D. 1999, MNRAS, 310, L5
Giacconi, R., et al. 2002, ApJS, 139, 369
Granato, G. L., Silva, L., Monaco, P., Panuzzo, P., Salucci, P., De Zotti, G., & Danese, L. 2001, MNRAS, 324, 757
Gruber, D. E., Matteson, J. L., Peterson, L. E., & Jung, G. V. 1999, ApJ, 520, 124
Haehnelt, M., Natarajan, P., & Rees, M. J. 1998, MNRAS, 300, 817
Haiman, Z., Ciotti, L., & Ostriker, J. P. 2004, ApJ, in press
Haiman, Z., & Loeb, A. 1998, ApJ, 503, 505
Hartwick, F. D. A., & Shade, D. 1990, ARA&A, 28, 437
Hasinger, G. 2003, in AIP Conf. Proc. 666, The Emergence of Cosmic Structure, ed. S. S. Holt & C. Reynolds (Melville: AIP), 227
Hatzminaoglou, E., Mathez, G., Solanes, J.-M., Manrique, A., & Salvador-Solé, E. 2003, MNRAS, 343, 692
Jenkins, A., Frenk, C. S., White, S. D. M., Colberg, J. M., Cole, S., Evrard, A. E., Couchman, H. M. P., & Yoshida, N. 2001, MNRAS, 321, 372
Kauffmann, G., & Haehnelt, M. 2000, MNRAS, 311, 576
———. 2002, MNRAS, 332, 529
Kauffmann, G., White, S. D. M., & Guiderdoni, B. 1993, MNRAS, 264, 201
Lacey, C., & Cole, S. 1993, MNRAS, 262, 627
Levine, A. M., et al. 1984, ApJS, 54, 581
Lumb, D. H., Warwick, R. S., Page, M., & De Luca, A. 2002, A&A, 389, 93
Madau, P., Ghisellini, G., & Fabian, A. C. 1994, MNRAS, 270, L17
Madau, P., & Rees, M. J. 2001, ApJ, 551, L27
Menci, N., Cavaliere, A., Fontana, A., Giallongo, E., & Poli, F. 2002, ApJ, 575, 18
Menci, N., Cavaliere, A., Fontana, A., Giallongo, E., Poli, F., & Vittorini, V. 2003, ApJ, 587, L63
———. 2004, ApJ, 604, 12
Mihos, C. 1999, Ap&SS, 266, 195
Mihos, J. C., & Hernquist, L. 1996, ApJ, 464, 641
Mo, H. J., Mao, S., & White, S. D. M. 1998, MNRAS, 295, 319
Monaco, P., Salucci, P., & Danese, L. 2000, MNRAS, 311, 279
Nulsen, P. E. J., & Fabian, A. C. 2000, MNRAS, 311, 346
Perola, G. C., Matt, G., Cappi, M., Fiore, F., Guainazzi, M., Maraschi, L., Petrucci, P. O., & Piro, L. 2002, A&A, 389, 802
Poli, F., et al. 2003, ApJ, 593, L1
Richstone, D., et al. 1998, Nature, 395, A14
Risaliti, G., Maiolino, R., & Salvati, M. 1999, ApJ, 522, 157
Sanders, D. B., & Mirabel, I. F. 1996, ARA&A, 34, 749
Setti, G., & Woltjer, L. 1989, A&A, 224, L21
Sheth, R. K., & Tormen, G. 1999, MNRAS, 308, 119
Silk, J., & Rees, M. J. 1998, A&A, 331, L1
Somerville, R. S., & Primack, J. R. 1999, MNRAS, 310, 1087
Tawara, Y., Kunieda, H., Inoue, H., Mitsuda, K., Ogasaka, Y., & Takahashi, T. 2003, Proc. SPIE, 4851, 324
Ueda, Y., Akiyama, M., Ohta, K., & Miyaji, T. 2003, ApJ, 598, 886
Vecchi, A., Molendi, S., Guainazzi, M., Fiore, F., & Parmar, A. N. 1999, A&A, 349, L73
Volonteri, M., Haardt, F., & Madau, P. 2003, ApJ, 582, 559
Wilman, R. J., & Fabian, A. C. 1999, MNRAS, 309, 862
Wu, K. K. S., Fabian, A. C., & Nulsen, P. E. J. 2000, MNRAS, 318, 889
Wyithe, J. S., & Loeb, A. 2002, ApJ, 581, 886
———. 2003, ApJ, 595, 614
Yu, Q., & Tremaine, S. 2002, MNRAS, 335, 965